Oxide ion conduction mechanism of $RE_{9.33}(SiO_4)_6O_2$ and $Sr_2RE_8(SiO_4)_6O_2$ (RE=La, Nd) from neutron powder diffraction

Yuji Masubuchi, Mikio Higuchi, Takashi Takeda and *Shinichi Kikkawa

Graduate School of Engineering, Hokkaido University, Sapporo 060-8628, Japan

PACS codes: 66.30.D, 61.66

Keywords: Oxide ion conductor, apatite-type structure, conduction mechanism, neutron diffraction, maximum entropy method

*Corresponding author

Fax: +81-(0)11-706-6739

E-mail: kikkawa@eng.hokudai.ac.jp

Abstract

Oxide ion conduction mechanism was clarified by Rietveld and MEM analysis for both $RE_{9.33}(SiO_4)_6O_2$ and $Sr_2RE_8(SiO_4)_6O_2$ (RE = La and Nd) in high purity using neutron powder diffraction data collected at room temperature. All compounds had an apatite type structure in space group $P6_3/m$. There was neither site splitting nor interstitial site of oxide ion. $RE_{9.33}(SiO_4)_6O_2$ had cation vacancies only at 4*f* site. In $Sr_2RE_8(SiO_4)_6O_2$, the 4*f* sites were fully occupied by strontium and rare earth with a molar ratio of 1:1. Oxide ion at hexagonal channel site had large displacement along c-axis in $RE_{9.33}(SiO_4)_6O_2$. The large displacement is induced by cooperative rotation of SiO_4 tetrahedra around rare earth in 4*f* site through oxide ion polyhedra around another rare earth in 6*h* site. The displacement, enhanced by a vacancy in the 4*f* site, is directly related to the oxide ion conduction in $RE_{9.33}(SiO_4)_6O_2$.

Introduction

Oxide ion conductors are very important for applications in solid oxide fuel cell and oxygen separator. Conventional oxide ion conductors have been stabilized zirconia with fluorite structure [1] and $La_{0.8}Sr_{0.2}Ga_{0.8}Mg_{0.15}Co_{0.05}O_{3-\delta}$ perovskite.[2] Nakayama et al. reported high oxide ion conductivity on rare earth silicates $RE_{9.33}(SiO_4)_6O_2$ with apatite structure.[3,4] The most attractive feature is that its conductivity at a relatively low temperature (below 600 °C) is much higher than that of stabilized zirconia. It has also reported that conduction in this compound is wholly ionic, with constant electrical conductivities across a wide range of oxygen partial pressure.[5] Single crystals had been grown for the $RE_{9.33}(SiO_4)_6O_2$ with RE=Pr, Nd and Sm by the floating zone method.[6-10] Their oxide ion conductivity was anisotropic, i.e. the conductivity parallel to c-axis in their hexagonal lattice was about one order of magnitude larger than that perpendicular to c-axis. The anisotropy in conduction was related to their crystal structure having open channel along c-axis (Fig. 1).

Another important feature is that $RE_{9.33}(SiO_4)_6O_2$ does not have oxide ion vacancy which had been essential for the conventional oxide ion conductors. It has vacancy of rare earth cation in 6.7%. Apatite structure in $P6_3/m$ has ten available sites for cations among both 4*f* and 6*h* sites in a unit cell. The vacancy is necessary to keep charge neutrality of the compound. In a recent computer modeling study, two kinds of oxide ion migration paths were proposed for $La_{9.33}(SiO_4)_6O_2$; one was a direct linear path through the hexagonal channel split sites and the other was a non-linear sinusoidal-like migration through a new interstitial oxide ion site.[12,13] An importance of SiO_4 units in the conduction process was firstly raised by this modeling, which indicated that the conduction process was aided by cooperative displacements of the silicate

substructure. Experimental doping studies had been performed to support this modeling on polycrystalline samples.[14]

Purity of the sample is very important for the structure analysis because $RE_{9.33}(SiO_4)_6O_2$ is easily contaminated either with RE_2SiO_5 or $RE_2Si_2O_7$. Masubuchi et al. applied both neutron powder diffraction and single crystal X-ray diffraction for the structure refinements on highly pure $Nd_{9.33}(SiO_4)_6O_2$ crystal. [11,15,16] A significantly large anisotropic displacement parameter parallel to c-axis was observed on the oxide ion in 2*a* site in the channel. The site splitting and interstitial site of oxide ion proposed by other investigators were not detected in the analysis. Single crystal X-ray diffraction for $La_{9.33}(SiO_4)_6O_2$ confirmed the above-mentioned results on structural analysis for the Nd-system in apatite structure (space group $P6_3/m$) with no symmetry lowering.[17] However the high oxide ion conduction mechanism generated by their cation vacancy in $RE_{9.33}(SiO_4)_6O_2$ has not yet been fully understood.

It is well known that the maximum entropy method (MEM) can be used to make electron or nuclear density distribution maps from a set of structural factors without the use of any structure model. Actually, there have been a number of studies on electron and nuclear density distribution using a combination of Rietveld refinement and the MEM. For example, ionic conduction path has been analyzed and well-visualized on Li^+ in $Li_{1-x}Ni_{0.5}Mn_{0.5}O_2$, O^{2-} in $(La_{0.8}Sr_{0.2})(Ga_{0.8}Mg_{0.15}Co_{0.05})O_{2.8}$. [18,19]

In the present study, the oxide ion conduction mechanism was discussed by visualizing nuclear density distribution map by the Rietveld and MEM analysis for both $RE_{9.33}(SiO_4)_6O_2$ and $Sr_2RE_8(SiO_4)_6O_2$ (RE = La and Nd) in high purity using neutron powder diffraction data collected at room temperature.

Experimental

High purity La_2O_3, Nd_2O_3, $SrCO_3$ and SiO_2 were used as the starting materials. They were mixed in ethanol with an agate mortar. The mixture was calcined at 1200 °C for 10 h and then sintered at 1650 °C for 20 h. The product was rubber-pressed under 100 MPa to discs after their grinding and sintered again at 1650 °C for another 20 h. Their phase purity was confirmed by powder X-ray diffraction (PHILIPS, X'pert-MPD). The sintered discs were about 9 mm in diameter and 1.5mm in thickness. Their both sides were coated with Pt paste as electrodes. Electrical conductivity was measured using AC impedance analyzer as described elsewhere.[4]

High purity samples are required for the reliable structure refinement. So that, $RE_{9.33}(SiO_4)_6O_2$ crystals were obtained by the floating zone method because of their congruent melting.[20] Neutron diffraction data was collected on powdered single crystals for $RE_{9.33}(SiO_4)_6O_2$. It was measured on as prepared powders for the other samples because they melted incongruently. [11]

These measurements were performed at room temperature with a wavelength of 0.182035 nm in the Kinken powder diffractometer HERMES installed at the JRR–3M reactor in Japan Atomic Energy Research Institute (JAERI), Tokai. The computer program RIETAN-2000 [21] was used for the structural refinement. Nuclear density distributions were analyzed using MEM program PRIMA. [22] Refined crystal structure and nuclear density images were visualized with a program VENUS [22] in three-dimension.

Structure refinements were carried out on the neutron powder diffraction data at room temperature similarly to our previous reports. [11] A space group of $P6_3/m$ was applied without site splitting of the conducting oxide ion. In the refinements of

$Sr_2RE_8(SiO_4)_6O_2$ (RE=La and Nd), a distribution of Sr and RE (molar ratio of 2:8) was employed for the two RE sites (4*f* and 6*h*) at the beginning. After convergence of their fractional coordinates, site occupancies of Sr and RE at the 4*f* and the 6*h* sites were refined.

Results and discussion

Electrical conductivity was measured on $RE_{9.33}(SiO_4)_6O_2$ and $Sr_2RE_8(SiO_4)_6O_2$ (RE = La and Nd) sintered compacts against temperature. $La_{9.33}(SiO_4)_6O_2$ showed the highest electrical conductivity among them as shown in Fig.2. Electrical conductivity of $Sr_2RE_8(SiO_4)_6O_2$ without cation vacancy was lower in about three orders of magnitudes than that of $RE_{9.33}(SiO_4)_6O_2$ with cation vacancy in the whole temperature range. The La-compounds had always higher electrical conductivity than the Nd-compounds whenever they had cation vacancies or not. Their conductivities changed almost linearly against T^{-1} following the Arrenius equation.

The finally refined parameters in Reitveld method are summarized in Table 1. Observed, calculated and their difference neutron diffraction profiles for $Sr_2Nd_8(SiO_4)_6O_2$ are shown in Fig. 3 as an example. The observation fits very well with the calculation. $RE_{9.33}(SiO_4)_6O_2$ has the cation vacancy concentration of 6.7%. All of the vacancies are present only at the RE1 (4*f*) site as shown in Table 1. The RE2 (6*h*) site is fully occupied by the rare earth elements, similarly to the previous reports.[11,15-17] For $Sr_2RE_8(SiO_4)_6O_2$, the RE1 site is fully occupied by both Sr and RE ions with a molar ratio of 1:1. There is no Sr ion at the RE2 site forming hexagonal channel. It is always occupied only by the rare earth ion similarly to the case in $RE_{9.33}(SiO_4)_6O_2$. These cation site occupancies suggest the channel structure is very similar among these

apatites. They are different only in whether they have cation vacancies or not at the RE1 site. The displacement parameters are anisotropic at the nine-coordinated RE1 site in the cation deficient compounds as shown in Table 2. This site is coordinated with 3×3 oxide ions in three O1, O2 and O3 sites belonging to SiO_4 tetrahedra as represented in Figs. 1 and 4(a). The RE1 site is anisotropic along c-direction, having some amount of vacancy.

No vacancy can be assumed on the channel oxide ion site O4 in its standard deviation for all samples as shown in Table 1. Displacement of O4 ion is anisotropically elongated along c-direction in all the present apatites. Degree of the anisotropy is different from sample to sample. $RE_{9.33}(SiO_4)_6O_2$ with cation vacancy has much larger anisotropy in its O4 displacement than $Sr_2RE_8(SiO_4)_6O_2$ without cation vacancy. The oxide ions have three-folds coordination with the rare earth ion at RE2 site in the same z-level (Fig. 1). They have displacement only along c-axis. The oxide ions migrate in the c-direction rather than a-directions. Their anisotropic displacement parameters at room temperature suggest that the oxide ion migration along c-axis would be enhanced at high temperature. In the cation deficient compounds, relatively large anisotropy was also observed on U_{11} of the O3 site as shown in Table 2 and Fig. 4(a). Figure 4(a) shows atomic arrangement around RE1 site for $La_{9.33}(SiO_4)_6O_2$ projected to (001). Oxide ions especially at O3 site around RE1 site with some amount of vacancy had the large displacement parameter due to their electrostatic repulsion against the cation vacancy because the cation vacancy has a negative formal charge.

The structure refinements indicate that the rare earth RE1 in 4*f* site seem to affect the motion of the oxide ions at the hexagonal channel as well as the rare earth RE2 in 6*h* site. Nuclear density images were drawn by MEM analysis in order to obtain

more detailed distribution of oxide ions. Figures 4(b) and (c) show the nuclear density images around RE1 site in $La_{9.33}(SiO_4)_6O_2$ and $Sr_2La_8(SiO_4)_6O_2$ at room temperature, respectively. Nuclear density distribution of oxide ions belonging to SiO_4 is broader especially at O1 and O3 for $La_{9.33}(SiO_4)_6O_2$ than those for $Sr_2La_8(SiO_4)_6O_2$. These distribution indicates that O1 and O3 are vibrating because there are electrostatic repulsions between the oxide ions and the formal negative charge on the RE1 site vacancy in $La_{9.33}(SiO_4)_6O_2$. The anisotropic displacement of O4 site for $La_{9.33}(SiO_4)_6O_2$ is ten times larger than that for $Sr_2La_8(SiO_4)_6O_2$. Both compounds have the RE2 site fully occupied only by lanthanum ions. The large vibration of the oxide ions also belonging to SiO_4 tetrahedra have a significant effect on oxide ion conduction at the hexagonal channel through the polyhedra around RE2. The cation vacancy results in a larger displacement of O4 channel site in $La_{9.33}(SiO_4)_6O_2$ than in $Sr_2La_8(SiO_4)_6O_2$. The slight rotation of the SiO_4 tetrahedron around RE1 induces the migration of oxide ions in O4 channel site through the coordination polyhedra around RE2. The vacancy in RE1 site enhances the oxide ion conduction along the channel because of the enhanced SiO_4 rotation. The oxide ion conduction occurs rather complicated way. It is not a direct linear path through the hexagonal channel split sites.

Nuclear density distributions were not much different in their size and shape between lanthanum and neodymium silicate as shown in Figs. 4(b) and (d). The lanthanum silicates had a little higher electrical conductivity than the neodymium silicates. Only a small difference in distribution among rare earth elements could be found using neutron diffraction measured at room temperature. High temperature neutron powder diffraction measurement will be planned to understand the oxide ion conduction mechanism and differences among the rare earth silicates at temperatures

where high conductivity has been observed.

With respect to the proposed cooperative effect of SiO_4 inducing displacement of channel oxide ions, there was no evidence for interstitial oxide ion. This mechanism implies that there must be such displacement of oxide ions into interstitial positions. Interstitial position has been proposed by the computer modeling work on polycrystalline samples. [13] Moreover, the thermal parameter U_{33}=0.32 for O4 is huge. This could not be classed as due to thermal motion, and strongly implies static displacements from the ideal 0,0,0.25 position. With respect to this, the present authors tried space group $P6_3$ but there was no improvement from $P6_3/m$. A number of interstitial oxide ion had been assumed to be present in the nominally stoichiometric samples. [23] Most of the present samples were powdered single crystals. Their stoichiometry is very strict. The displacement suggested by the MEM analysis is indeed an evidence for their thermal motion of oxide ions in this position.

In summary, crystal structures and nuclear density distributions of $RE_{9.33}(SiO_4)_6O_2$ and $Sr_2RE_8(SiO_4)_6O_2$ (RE=La, Nd) were studied using Rietveld analysis of neutron powder diffraction data and the maximum entropy method. Structure analysis indicated that all the compounds adopt space group $P6_3/m$. There were no site splitting of the channel and interstitial oxide ions suggested in the previous manuscripts. [12] RE1-4*f* site was occupied by rare earth ions with some amount of cation vacancy in $RE_{9.33}(SiO_4)_6O_2$. It was fully occupied by rare earth and strontium ions in $Sr_2RE_8(SiO_4)_6O_2$. Oxide ions at hexagonal channel had anisotopic displacement along c-axis in all the samples. This anisotropy was much larger in $RE_{9.33}(SiO_4)_6O_2$ having cation vacancy. Cation vacancy in RE1 site enhanced the oxide ions displacement belonging to SiO_4. The slight rotation of SiO_4 tetrahedra cooperatively induced an

anisotropic displacement of the channel oxide ions along c-axis through the polyhedra around the rare earth RE2-6*h* site. The SiO_4 rotations induce displacements in the channel oxide ions and hence the large U_{33}, and therefore encourage the conduction.

Acknowledgement

Authors would like to thank Drs. T. Wakeshima and Y. Hinatsu in Hokkaido University for neutron diffraction data acquisition.

References

[1] A. Brune, M. Lajavardi, D. Fisler and J.B. Wagner Jr., *Solid State Ionics* **1998**, *106*, 89.

[2] K. Kuroda, I. Hashimoto, K. Adachi, J. Akikusa, Y. Tamou, N. Komada, T. Ishihara and Y. Takita, *Solid State Ionics* **2000**, *132*, 199.

[3] S. Nakayama, T. Kageyama, H. Aono and Y. Sadaoka, *J. Mater. Chem.* **1995**, *5*, 1801.

[4] S. Nakayama and M. Sakamoto, *J. Eur. Ceram. Soc.* **1998**, *18*, 1413.

[5] H. Arikawa, H. Nishiguchi, T. Ishihara and Y. Takita, *Solid State Ionics* **2000**, *136-137*, 31.

[6] S. Nakayama, M. Sakamoto, M. Higuchi, K. Kodaira, M. Sato, S. Kakita, T. Suzuki and K. Itoh, *J. Eur. Ceram. Soc*. **1999**, *19*, 507.

[7] M. Higuchi, K. Kodaira and S. Nakayama, *J. Crystal Growth* **1999**, *207*, 298.

[8] S. Nakayama, M. Sakamoto, M. Higuchi and K. Kodaira, *J. Mater. Sci. Lett.* **2000**, *19*, 91.

[9] M. Higuchi, K. Kodaira and S. Nakayama, *J. Crystal Growth* **2000**, *216*, 317.

[10] M. Higuchi, H. Katase, K. Kodaira and S. Nakayama, *J. Crystal Growth* **2000**, *218*, 282.

[11] Y. Masubuchi, M. Higuchi, H. Katase, T. Takeda, S. Kikkawa, K. Kodaira and S. Nakayama, *Solid State Ionics* **2004**, *166*, 213.

[12] J. E. H. Sansom, D. Richings, P. R. Slater, *Solid State Ionics* **2001**, *139*, 205.

[13] J. R. Tolchard, M. S. Islam and P. R. Slater, *J. Mater. Chem.* **2003**, *13*, 1956.

[14]A. Najib, J. E. H. Sansom, J. R. Tolchard, P. R. Slater and M. S. Islam, Dalton Trans. **2004**, 3106.

[15] H. Okudera, A. Yoshiasa, Y. Masubuchi, M. Higuchi and S. Kikkawa, *Zeitschrift fur Kristallographie* **2004**, *219*, 27.

[16] H. Okudera, A. Yoshiasa, Y. Masubuchi, M. Higuchi and S. Kikkawa, *J. Solid State Chem.* **2004**, *177*, 4451.

[17] H. Okudera, Y. Masubuchi, S. Kikkawa and A. Yoshiasa, *Solid State Ionics*, in press.

[18] H. Kobayashi, Y. Arachi, H. Kageyama and K. Tatsumi, *J. Mater. Chem.* **2004**, *14*, 40.

[19] M. Yashima, K. Nomura, H. Kageyama, Y. Miyazaki, N. Chitose and K. Adachi, *Chem. Phys. Lett.* **2003**, *380*, 391.

[20] Y. Masubuchi, M. Higuchi and K. Kodaira, *J. Crystal Growth* **2003**, *247*, 207.

[21] F. Izumi and T. Ikeda, *Mater. Sci. Forum* **2000**, *198* 321.

[22] F. Izumi and R. A. Dilanian, *Recent Research Developments in Physics*, Vol. 3, Transworld Research Network, Trivandrum, **2002**, 669.

[23] L. León-Reina, E. R. Losilla, M. Martínez-Lara, S. Bruque and M. A. G. Aranda, J. Mater. Chem. **2004**, *14*, 1142.

Figure and table captions

Figure 1. Crystal structure of apatite-type rare earth silicate.[11] The oxide ions in the channel structure are coordinated with rare earth cations at RE-6*h* sites.

Figure 2. Temperature dependence of electrical conductivities for sintered samples: ○ $La_{9.33}(SiO_4)_6O_2$; ● $Sr_2La_8(SiO_4)_6O_2$; □ $Nd_{9.33}(SiO_4)_6O_2$; ■: $Sr_2Nd_8(SiO_4)_6O_2$.

Figure 3. Observed (+), calculated (solid line) and their difference profiles on powder neutron diffraction for $Sr_2Nd_8(SiO_4)_6O_2$.

Fig. 4 (a); Atomic arrangement around RE1-4*f* site for $La_{9.33}(SiO_4)_6O_2$. The ellipsoid represents the anisotropic displacement. Equicontour surfaces of nuclear scattering amplitude (0.5 fm/Å) around RE1 site are projected to (001) plane in (b) $La_{9.33}(SiO_4)_6O_2$, (c) $Sr_2La_8(SiO_4)_6O_2$ and (d) $Nd_{9.33}(SiO_4)_6O_2$.

Table 1. Refined structural parameters for $RE_{9.33}(SiO_4)_6O_2$ and $Sr_2RE_8(SiO_4)_6O_2$ (RE = La and Nd) at room temperature.

Table 2. Refined anisotropic displacement parameters for $RE_{9.33}(SiO_4)_6O_2$ and $Sr_2RE_8(SiO_4)_6O_2$ (RE = La and Nd) at room temperature.

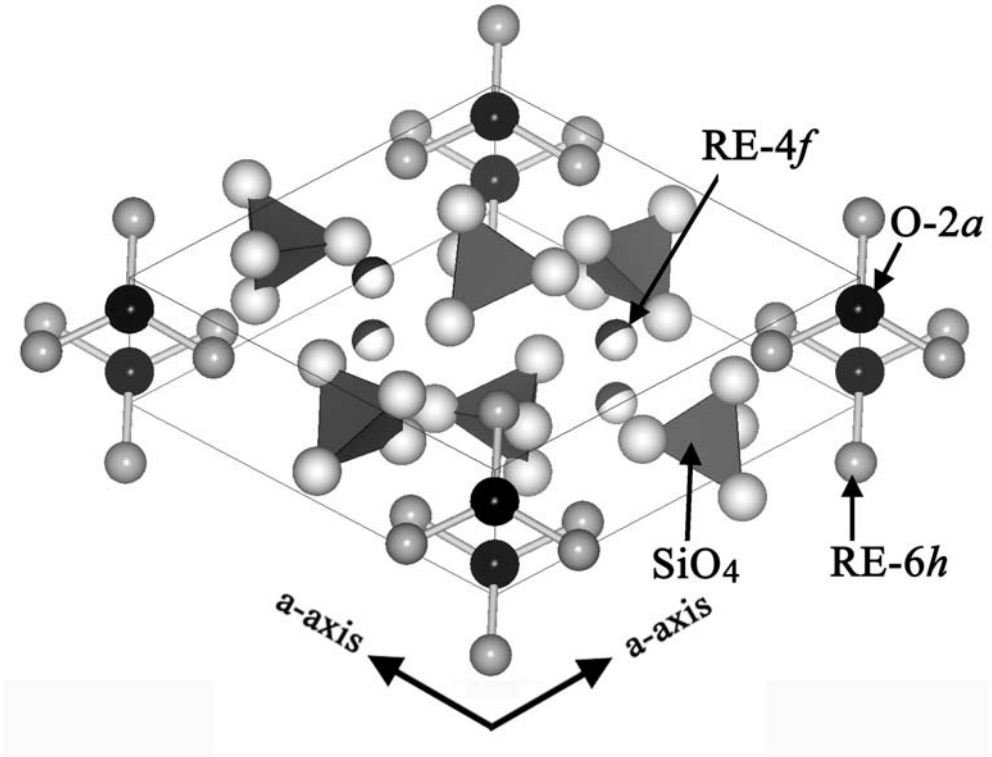

Figure 1. Crystal structure of apatite-type rare earth silicate.[11] The oxide ions in the channel structure are coordinated with rare earth cations at RE-6*h* sites.

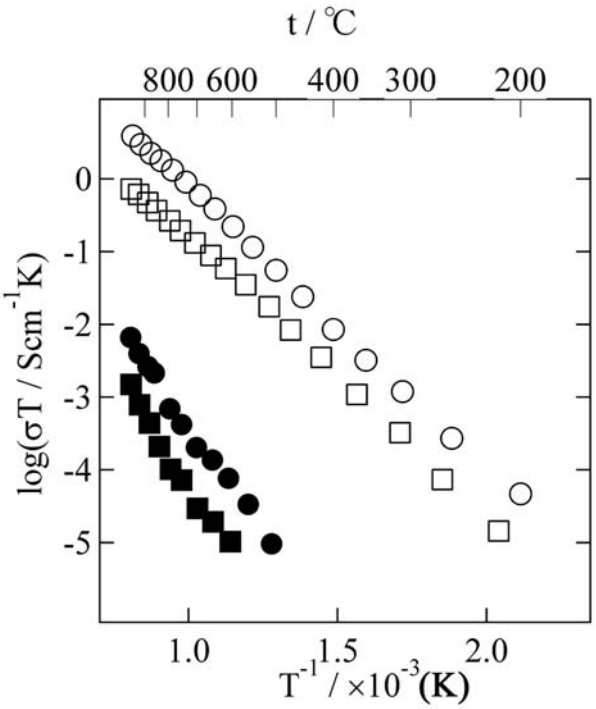

Figure 2. Temperature dependence of electrical conductivities for sintered samples: ○ $La_{9.33}(SiO_4)_6O_2$; ● $Sr_2La_8(SiO_4)_6O_2$; □ $Nd_{9.33}(SiO_4)_6O_2$; ■: $Sr_2Nd_8(SiO_4)_6O_2$.

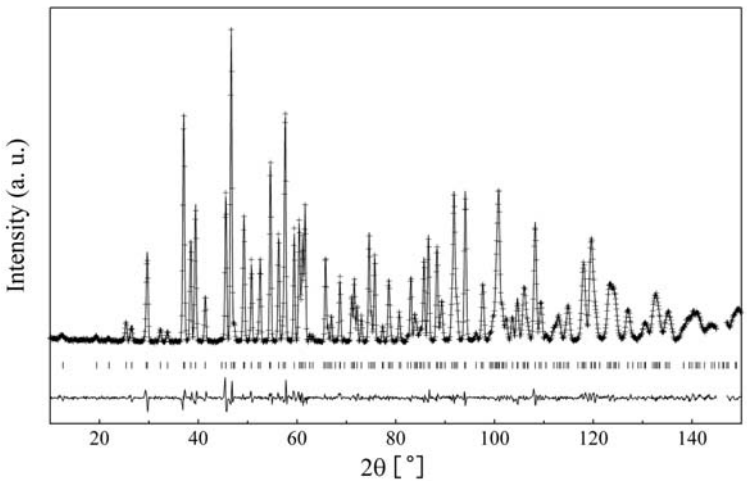

Figure 3. Observed (+), calculated (solid line) and their difference profiles on powder neutron diffraction for $Sr_2Nd_8(SiO_4)_6O_2$.

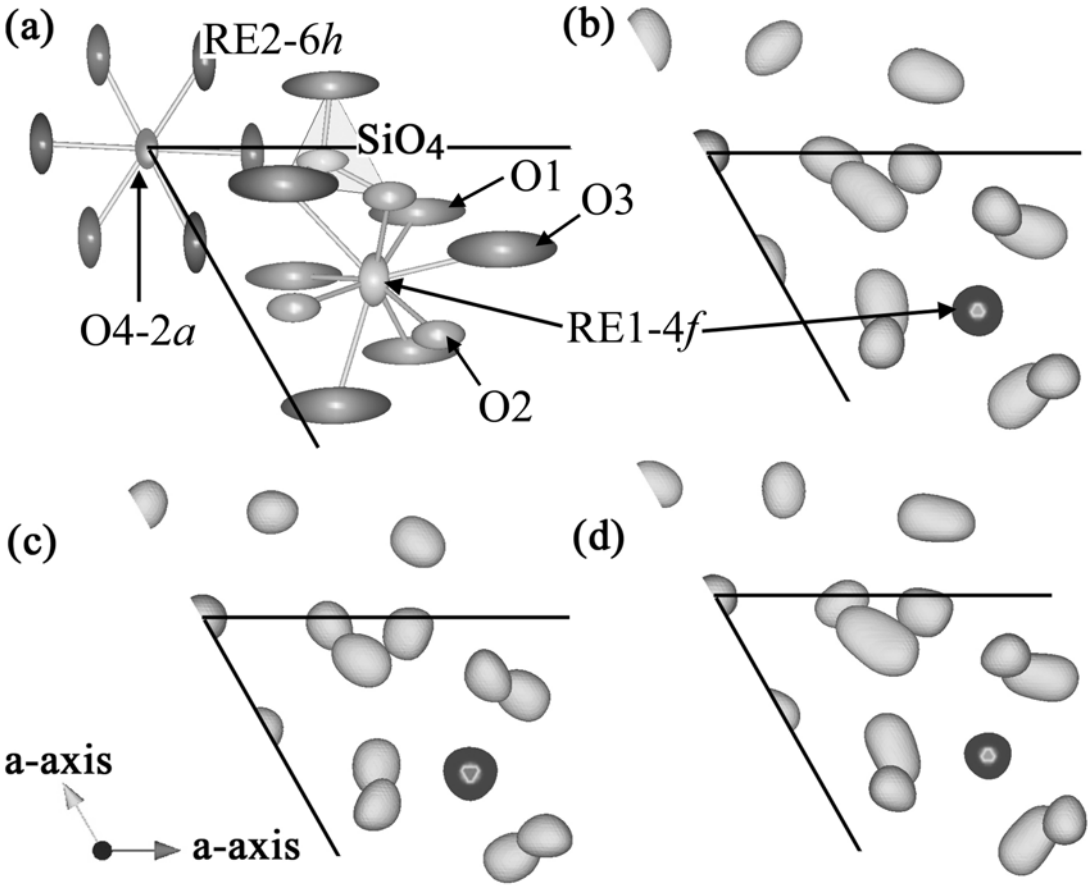

Fig. 4 (a); Atomic arrangement around RE1-4*f* site for $La_{9.33}(SiO_4)_6O_2$. The ellipsoid represents the anisotropic displacement. Equicontour surfaces of nuclear scattering amplitude (0.5 fm/Å) around RE1 site are projected to (001) plane in (b) $La_{9.33}(SiO_4)_6O_2$, (c) $Sr_2La_8(SiO_4)_6O_2$ and (d) $Nd_{9.33}(SiO_4)_6O_2$.

Table 1. Refined structural parameters for $RE_{9.33}(SiO_4)_6O_2$ and $Sr_2RE_8(SiO_4)_6O_2$ (RE = La and Nd) at room temperature.

Compounds	$La_{9.33}(SiO_4)_6O_2$	$Sr_2La_8(SiO_4)_6O_2$	$Nd_{9.33}(SiO_4)_6O_2$	$Sr_2Nd_8(SiO_4)_6O_2$
a / nm	0.97228(1)	0.97048(1)	0.95690(1)	0.95666(1)
c / nm	0.71881(1)	0.72411(1)	0.70225(1)	0.71062(1)
RE1/Sr1, 4*f*, (1/3, 2/3, *z*)				
z	-0.0003(5)	-0.0007(4)	0.0000(6)	-0.0004(3)
site occ. (RE/Sr)	0.84(8)/0.0	0.49(3)/0.51(3)	0.85(6)/0.0	0.50(1)/0.50(1)
RE2/Sr2, 6*h*, (*x*, *y*, 1/4)				
x	0.0130(3)	0.0144(2)	0.0105(3)	0.0107(2)
y	0.2389(2)	0.2454(2)	0.2406(3)	0.2422(2)
site occ. (RE/Sr)	0.995(6)/0.0	0.99(3)/0.00(3)	1.00(1)/0.0	1.00(4)/0.00(4)
Si, 6*h*, (*x*, *y*, 1/4)				
x	0.4020(5)	0.3994(4)	0.4008(6)	0.3985(4)
y	0.3713(4)	0.3696(4)	0.3713(6)	0.3694(4)
O1, 6*h*, (*x*, *y*, 1/4)				
x	0.3241(4)	0.3224(3)	0.3219(5)	0.3163(3)
y	0.4854(4)	0.4839(3)	0.4867(5)	0.4818(4)
O2, 6*h*, (*x*, *y*, 1/4)				
x	0.5949(3)	0.5933(4)	0.5950(4)	0.5947(3)
y	0.4739(4)	0.4707(3)	0.4728(5)	0.4739(3)
O3, 12*i*, (*x*, *y*, *z*)				
x	0.3456(3)	0.3409(2)	0.3447(3)	0.3403(2)
y	0.2562(3)	0.2525(2)	0.2539(3)	0.2504(3)
z	0.0698(2)	0.0695(2)	0.0675(3)	0.0672(2)
O4, 2*a*, (0, 0, 1/4)				
site occ.	1.00(1)	0.99(2)	1.00(1)	0.99(1)
R_{wp} (%)	5.57	5.20	5.64	3.99
R_p (%)	4.26	3.78	4.38	2.98
R_e (%)	2.68	2.27	2.96	2.08

Table 2. Refined anisotropic displacement parameters for $RE_{9.33}(SiO_4)_6O_2$ and $Sr_2RE_8(SiO_4)_6O_2$ (RE = La and Nd) at room temperature.

Compounds	$La_{9.33}(SiO_4)_6O_2$	$Sr_2La_8(SiO_4)_6O_2$	$Nd_{9.33}(SiO_4)_6O_2$	$Sr_2Nd_8(SiO_4)_6O_2$
RE1/Sr1, 4*f*, $U_{22}=U_{11}=2U_{12}$, $U_{13}=U_{23}=0$				
U_{11} / $\times 10^{-2}$nm^2 (=Å^2)	0.009(1)	0.011(1)	0.004(1)	0.010(1)
U_{33}	0.018(2)	0.002(1)	0.023(2)	0.008(1)
RE2/Sr2, 6*h*, $U_{13}=U_{23}=0$				
U_{11}	0.005(1)	0.006(1)	0.003(1)	0.008(1)
U_{22}	0.016(1)	0.006(1)	0.003(1)	0.003(1)
U_{33}	0.008(1)	0.007(1)	0.005(1)	0.007(1)
U_{12}	0.006(1)	0.005(1)	-0.001(1)	0.002(1)
Si, 6*h*, $U_{13}=U_{23}=0$				
U_{11}	0.010(2)	0.005(2)	0.011(1)	0.003(1)
U_{22}	0.006(5)	0.009(4)	0.006(1)	0.007(2)
U_{33}	0.018(2)	0.010(2)	0.018(2)	0.014(2)
U_{12}	0.005(2)	0.002(1)	0.007(1)	0.003(1)
O1, 6*h*, $U_{13}=U_{23}=0$				
U_{11}	0.030(2)	0.017(2)	0.040(3)	0.017(1)
U_{22}	0.020(3)	0.007(2)	0.031(3)	0.016(2)
U_{33}	0.011(2)	0.011(2)	0.014(3)	0.019(2)
U_{12}	0.021(2)	0.002(1)	0.029(2)	0.012(1)
O2, 6*h*, $U_{13}=U_{23}=0$				
U_{11}	0.011(2)	0.007(1)	0.004(2)	0.009(1)
U_{22}	0.007(2)	0.001(1)	0.016(2)	0.012(1)
U_{33}	0.033(3)	0.014(2)	0.013(2)	0.019(1)
U_{12}	0.004(1)	-0.001(1)	0.007(1)	0.006(1)
O3, 12*i*				
U_{11}	0.048(2)	0.023(1)	0.063(2)	0.021(1)
U_{22}	0.014(2)	0.010(1)	0.020(1)	0.014(1)
U_{33}	0.015(1)	0.013(1)	0.008(1)	0.013(1)
U_{12}	0.017(1)	0.011(1)	0.023(2)	0.010(1)
U_{13}	-0.014(1)	-0.004(1)	-0.014(1)	-0.006(1)
U_{23}	-0.006(1)	-0.004(1)	-0.001(1)	-0.003(1)
O4, 2*a*, $U_{11}=U_{22}=2U_{12}$, $U_{13}=U_{23}=0$				
U_{11}	0.005(2)	0.010(1)	0.008(2)	0.013(1)
U_{33}	0.32(1)	0.034(3)	0.103(8)	0.026(3)